JCTC Journal of Chemical Theory and Computation

ProMetCS: An Atomistic Force Field for Modeling Protein−Metal Surface Interactions in a Continuum Aqueous Solvent

Daria B. Kokh,*,† Stefano Corni,‡ Peter J. Winn,§ Martin Hoefling,|| Kay E. Gottschalk,|| and Rebecca C. Wade*,†

Molecular and Cellular Modeling Group, Heidelberg Institute for Theoretical Studies (HITS gGmbH), Schloss-Wolfsbrunnenweg 35, D-69118 Heidelberg, Germany, INFM-CNR National Research Center on nanoStructures and BioSystems at Surface (S3), Modena, Italy, Centre for Systems Biology, School of Biosciences, The University of Birmingham, Edgbaston, Birmingham, B15 2TT, United Kingdom, and Ludwig Maximilians University, Munich, German

Received February 12, 2010

Abstract: In order to study protein−inorganic surface association processes, we have developed a physics-based energy model, the ProMetCS model, which describes protein−surface interactions at the atomistic level while treating the solvent as a continuum. Here, we present an approach to modeling the interaction of a protein with an atomically flat Au(111) surface in an aqueous solvent. Protein−gold interactions are modeled as the sum of van der Waals, weak chemisorption, and electrostatic interactions, as well as the change in free energy due to partial desolvation of the protein and the metal surface upon association. This desolvation energy includes the effects of water−protein, water−surface, and water−water interactions and has been parametrized using molecular dynamics (MD) simulations of water molecules and a test atom at a gold−water interface. The proposed procedure for computing the energy terms is mostly grid-based and is therefore efficient for application to long-time simulations of protein binding processes. The approach was tested for capped amino acid residues whose potentials of mean force for binding to a gold surface were computed and compared with those obtained previously in MD simulations with water treated explicitly. Calculations show good quantitative agreement with the results from MD simulations for all but one amino acid (Trp), as well as correspondence with available experimental data on the adhesion properties of amino acids.

1. Introduction

Protein−surface binding events are of great importance in many bioengineering, biomedical and nanotechnology applications. For example, protein adsorption properties are crucial for the integration of medical implants with tissue, and for the assembly of interfacial protein constructs in nanotechnology, such as sensors, activators, and other functional components at the biological/electronic junction. Over the past decades, extensive experimental investigations on the molecular recognition, binding, and self-assembly of proteins, peptides, and amino acids on inorganic surfaces have been reported (for gold, see refs 1−7), and even combinatorially selected peptides with affinity for specific inorganic materials have been successfully synthesized.[8−10] For some examples of protein adsorption studies, particularly in connection with possible applications, see the reviews in refs 11−14 and references therein.

Because of the high complexity of protein adsorption phenomena and the scarcity of experimental data at the

* Corresponding author e-mail: daria.kokh@h-its.org (D.B.K.) and rebecca.wade@h-its.org (R.C.W.).
† Heidelberg Institute for Theoretical Studies.
‡ INFM-CNR National Research Center.
§ The University of Birmingham.
|| Ludwig Maximilians University.

10.1021/ct100086j
Published on Web 04/16/2010

atomistic level, however, the mechanisms by which biomolecules interact with inorganic surfaces are still poorly understood,[14] and until very recently, investigations of protein adsorption properties either had a rather qualitative character or were done on the macroscopic scale. This is why, in recent years, great efforts have been applied to adapt computational methods that are usually employed for molecular modeling in solution to the protein−surface problem. In particular, all-atom empirical force field methods, treating water molecules and the internal coordinates of an adsorbate explicitly, are now widely used to investigate biomolecule−surface binding behavior at the atomistic level[13−24] and have been shown to be able to provide qualitative agreement with experimentally observed adsorption tendencies for some small peptides.[19] However, all-atom molecular modeling methods, with explicit inclusion of water molecules, are extremely computationally demanding and therefore restricted to short time (typically of 10−100 ns) and length scales, while most experimental studies give an averaged behavior of large biomolecules over milliseconds or longer. Most of the atoms in molecular dynamics (MD) simulations with explicit water molecules come from the solvent itself. Furthermore, the presence of explicit water molecules slows protein motions. These two factors can make the computational time needed for the convergence of calculated properties extremely long. Therefore, a possible way to reduce computational time is to use an implicit solvent model that, in combination with an all-atom force field representation of a protein, may provide a reasonable compromise between accuracy and computational cost.

Existing implicit solvent models have primarily been developed for simulation of protein or peptide behavior in solution alone[25] and are generally not appropriate for protein interactions with inorganic interfaces.[13] This was demonstrated, in particular, by Sun and Latour[26] in their comparative analysis of commonly used empirical force-field-based implicit solvent models. It was found that the adsorption free energy of a peptide on a self-assembled monolayer (SAM) may change by up to several tens of kilocalories per mole, depending on which solvent model was used for the calculations. Furthermore, it has been recognized recently that the microscopic properties of the hydration shell vary for different solid surfaces, thereby altering the mechanism of adsorbate−surface interaction. For example, on metal surfaces, the desolvation energy may cause a transition barrier to adsorption due to the energetically unfavorable displacement of the water layer,[24] whereas, for some polar surfaces, peptides may be bound to the structured water layer rather than to the surface itself.[23] Hence, to provide a reliable description of protein−metal association in aqueous solvent, the solvent model should include a microscopic characterization of processes at the protein−surface interface.

In the present paper, we propose an approach for computation of the adsorption free energy of a biomolecule to a gold surface with an implicit solvent model that accounts for the short- and long-range effects of the protein−solvent−metal interactions. We employed the Au(111) surface for modeling because of its importance in the field of protein−surface interactions, both for fundamental studies (well-characterized, stable surface in both air and water) and for potential applications (e.g., contacts in nanobioelectronics and optical detection systems). Moreover, extensive theoretical investigations of small organic molecules adsorbed on gold,[1,7,20,27−29] as well as experimental data on protein and peptide adsorption,[3,5,7] are available and can be used for model optimization and validation. The present energy function is designed for use in Brownian Dynamics (BD) simulations of protein adsorption to surfaces but is not limited to this application.

BD methods in which solute molecules are treated as rigid bodies diffusing in a continuum solvent are commonly applied to simulate diffusion-influenced reactions and have been shown to be successful for computing protein−protein,[30] protein−small molecule,[31] and protein−membrane[32] association kinetics. Similarly, BD methods can be directly applied to a large group of proteins with high internal stability that can adsorb onto inorganic surfaces without appreciable changes in conformation or can form a transient complex before conformational changes occur. This method may also open the way for simulation of protein−protein interactions mediated by solid surfaces or protein self-assembly on inorganic substrates.

Despite the apparent similarity of the protein−protein and protein−solid surface association reactions, they have intrinsic differences in kinetics and in the driving forces for the binding processes. Indeed, the leading interaction in the case of protein−protein association to a diffusional encounter complex often arises from the long-range electrostatic forces, while the short-range effects can be described simply by prohibiting overlap of the exclusion volumes of the proteins. The influence of electrostatics on the interaction between a protein and an uncharged metal surface is much weaker since it arises solely from polarization effects. For a neutral solute molecule without a well-pronounced dipole moment, the image-charge potential must rapidly converge to zero as the distance from the metal increases due to the cancellation of contributions from opposite charges. On the other hand, at small distances from the surface, short-range interactions such as van der Waals forces and small metal−solute molecule charge transfers (that may also involve π electrons), along with the desolvation free energy, dominate over the electrostatic interaction. The construction of such an energy function is facilitated by the fact that the van der Waals interaction between organic molecules and a solid state surface, in particular gold, has recently been parametrized with a set of force field parameters[27] which can be directly implemented at an atomistic level in the energy function. A continuum solvent model able to provide a reliable description of the solvent−protein−solid interface, especially hydrophobic effects, needs to be developed and parametrized. This task is complicated by the fact that there is no well-established microscopic model of the protein−water−metal interface even though the behavior of aqueous solvent itself on the metal (in particular, gold) surfaces has been intensively studied both theoretically[33−40] and experimentally,[33,41−45] and some solution-driven effects in MD simulations of peptide adsorption on metal surfaces have been reported.[19,23,24]

In experimental studies of metal wetting properties, gold surfaces have been described both as hydrophilic (on the basis of contact angle measurements)[43] and rather hydrophobic (from the sublimation kinetics of ice layers).[45] On the other hand, experimental and theoretical evidence indicates that water−Au(111) interactions are weak relative to the hydrogen bonds between water molecules.[33,34,40] To minimize the intermolecular interaction energy in the interfacial region at an uncharged surface, water forms hydrogen-bonded clusters (in some studies described as having an ice-like structure[40,42,44]) in which the water dipoles in contact with the metal surface are oriented in the surface plane or slightly tilted with hydrogen oriented toward the bulk water (oxygen points to the surface).[33,42] MD simulations and *ab initio* calculations show that the water density has a maximum in the vicinity of the Au(111) surface (the first water layer) and some density fluctuations at larger distances caused by screening effects (the hydration shell).[34,37−40] This effect is responsible for some energy penalty due to displacement of the hydration shell upon adsorption, which makes binding to gold in water less favorable than in a vacuum as observed in MD simulations.[24] Furthermore, oriented water molecules on the metal surface, acting as dipoles, induce an electrostatic field, which may affect the behavior of charged and polar molecules.[39] Taking all these data into account, it is reasonable to include in the continuum solvent model both the hydrophobic and the electrostatic effects of the interaction with the hydration shell of the metal, and to employ MD simulations of water molecules to compute their hydrophobic and electrostatic contributions to the desolvation energy, in order to parametrize them.

Finally, to check the designed continuum solvent model, we need a well-characterized test system that not only allows us to verify the reliability of our representation of solvation effects and the derived energy parameters but also helps us to understand the contributions of different interaction mechanisms to the total protein−metal binding free energy. It is reasonable therefore to start with validation on small systems, whose interaction can be studied accurately either by experimental or by theoretical methods or both, and then make use of parameter transferability to apply the method to larger ones. The natural choice of such small systems is a set of amino acids whose binding to metal surfaces has been analyzed using MD simulations[28,29] and can also be related to available experimental studies.[1,5,7,9] For the sake of consistency, we used the same gold surface representation, amino acid structures, and force field parameters as used previously in the MD simulations.[28,29] We also employed the same image-charge model and water force field in the MD simulations with explicit water molecules performed to support the development of the continuum approach presented here. Thus, we note that the ProMetCS model developed is based on the force field employed in MD simulations (the GolP model[27]) and, therefore, inherits the limitations of the latter.

The paper is organized as follows. In the next section (Computational Methods), we describe the procedure used for calculating adsorption free energy. We show how the effects of solvent−metal−solute interactions can be approximated by physics-based energy terms, parametrized using explicit solvent simulations, and how they are implemented in the ProMetCS model. We give details of the MD simulations of the behavior of water molecules in the metal hydration shell, which we have used for the design and parametrization of the desolvation energy term. Finally, we show how the adsorption free energy and the potential of mean force (PMF) obtained from MD simulations can be calculated with the ProMetCS model. In the following section, we present the results of the application of the ProMetCS model to amino acid residues and compare the computed PMF binding energies with those from MD simulations as well as with available experimental data. In Appendix I, we give details of the MD simulations of the behavior of water molecules and test atoms in the surface hydration shell that were used for the design and parametrization of the desolvation energy. In Appendix II, we estimate the influence of the intrinsic electrostatic field of the hydration shell on the adsorption of charged molecules.

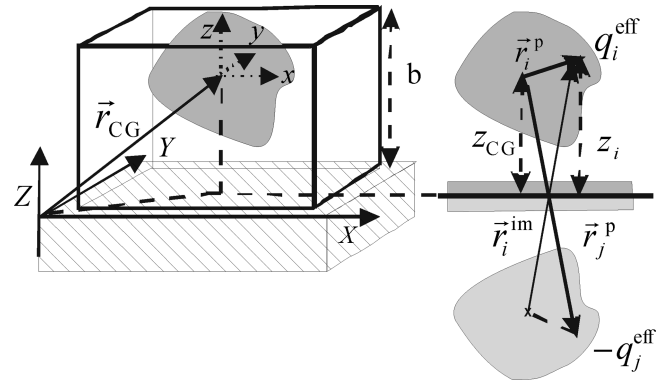

Figure 1. Illustration of the simulation box used for the calculations (left panel) and of the protein-image system employed for computing metal polarization effects (right panel). The low dielectric cavities of the protein and surface are shaded dark gray, and their images are light gray. The gold cluster is shown by a hatched block. Vectors are defined as $\vec{r}_j^{\,p} \equiv (x_i^p, y_i^p, -z_i^p - 2z_{CG})$ and $\vec{r}_i^{\,im} \equiv (x_i^p, y_i^p, z_i^p + 2z_{CG})$ from the geometric centers of the real and image protein, respectively. z_{CG} is the distance between the geometric center of the protein and the surface, and $z_i \equiv z_{CG} + z_i^p$ is the distance between a protein effective charge *i* and the surface.

2. Computational Methods

2.1. Description of System (Setup). The Au(111) surface is described by a gold cluster with atomic layers. A minimum of three layers is necessary (and sufficient) for the accurate calculation of protein−gold van der Waals interactions, as will be shown below. During the calculations, the position of the cluster is fixed with the centers of the atoms in the surface layer at $z = 0$, i.e., in the xy plane of the simulation box, as illustrated in Figure 1. The surface area of the cluster must be larger than the size of the adsorbate in order to account for interatomic interaction effects up to the cutoff employed in calculations (see below). In the present study, a gold cluster with surface dimensions of 100 Å × 100 Å was employed. Since we used the force field parameters for the biomolecule−gold interaction derived in ref 27, the cluster was constructed accordingly (see details below). In

calculations of electrostatic and desolvation effects, the gold surface was considered to be a plane.

A distance b from the surface defines the limit of the simulation box where the protein−surface interaction energy is negligible and serves as a reference state for the calculation of the protein adsorption free energy and PMFs. The $z = b$ plane is also used for the generation of the starting positions of the adsorbate for the computation of BD trajectories.

Amino acid residues capped with an acetyl group at the N terminus and a methylamide group at the C terminus, corresponding to those studied in refs 28 and 29, were employed as test adsorbates. Calculations were performed for all 20 natural amino acids with their side chains assigned the standard protonation state at pH 7. Cysteine is known to form a strong bond with the gold surface which cannot be described by the Lennard-Jones-based force field parameters and a rigid gold surface. Therefore, we considered only the protonated form (denoted CysH), which cannot form a strong bond to gold, for the present simulations. To evaluate the effect of conformational variability of the capped amino acids upon binding to gold, we compared the binding properties of several of the most populated binding conformations obtained in MD simulations.[28]

2.2. Implicit Solvent Model: Interaction Energy Function. The protein−metal interaction energy function, U, which implicitly includes solvent effects, is expressed in the ProMetCS model as a sum of three separate contributions:

$$U = E_{\mathrm{LJ}} + U_{\mathrm{EP}} + U_{\mathrm{desolv}} \tag{1}$$

The E_{LJ} energy term describes nonpolar, van der Waals, and weak chemical interactions between a protein and a metal surface. It is parametrized to reproduce experimental binding properties of small organic molecules on gold.[27] It is a sum of classical Lennard-Jones 12−6 terms and will hereafter be denoted as a Lennard-Jones (LJ) term.

U_{EP} is the protein−metal electrostatic interaction free energy in aqueous solvent. (In the general case, it also includes the energy due to the electrostatic interaction between the charges in the protein binding site and the interfacial water potential on the metal surface, see Appendix II; this latter term is neglected in the implementation described in this work.)

The last term in eq 1, U_{desolv}, describes desolvation effects, i.e., the free energy change arising from protein−water, solid surface−water, and water−water interactions. Desolvation effects can be further split into two separate components: the desolvation energy of the protein, $U^{\mathrm{p}}_{\mathrm{desolv}}$, and the desolvation energy of the metal surface, $U^{\mathrm{m}}_{\mathrm{desolv}}$:

$$U_{\mathrm{desolv}} = U^{\mathrm{p}}_{\mathrm{desolv}} + U^{\mathrm{m}}_{\mathrm{desolv}} \tag{2}$$

The first term, the nonpolar (or hydrophobic) protein desolvation energy, is the free energy change of the protein−water system that arises from the replacement of the protein−water interface in the region of the adsorption site by a protein−vacuum interface. The second term in eq 2 represents effects arising from the partial replacement of the metal hydration shell by a protein adsorption site and is given by the free energy change due to insertion of a hydrophobic cavity (which mimics the binding site of the protein) into the hydration shell of the metal surface (note that the change of the protein−metal electrostatic interaction due to surface desolvation is instead included in the electrostatic energy term, U_{EP}).

It should be noted that the entropy contribution to the function represented by eq 1 [specifically, the second and third terms] is limited to the entropy change upon binding of the solvent only. The entropy change due to the restriction of protein motion upon binding the metal surface must be calculated separately. Hence, although U in eq 1 includes some entropic effects, it does not correspond to the complete adsorption free energy. The procedure for calculation of the entire adsorption free energy will be considered at the end of the present section. The three terms contributing to U in eq 1 are now described in more detail.

2.2.1. Lennard-Jones Term: E_{LJ}. van der Waals and weak chemical interactions between the biomolecule and the gold surface are described by the sum of 12−6 Lennard-Jones atom−atom pair potentials corresponding to interactions between each atom i of the biomolecule and each atom j of the gold cluster

$$E_{\mathrm{LJ}} = \sum_j \sum_i 4\varepsilon_{ij}[(\sigma_{ij}/R_{ij})^{12} - (\sigma_{ij}/R_{ij})^{6}] \tag{3}$$

where R_{ij} is the interatomic distance and

$$\varepsilon_{ij} = \sqrt{\varepsilon_{ii}\varepsilon_{jj}} \text{ and } \sigma_{ij} = \sqrt{\sigma_{ii}\sigma_{jj}}$$

are the (OPLS/AA-like) gold force field (GolP) parameters optimized by Iori et al.[27] for the interaction between organic molecules and a Au(111) surface.

The most important additions introduced in the GolP force field with respect to the standard OPLS/AA force-field[46] can be briefly summarized as follows: (i) The physical position of each Au atom in the upper layer of the gold cluster was replaced by two virtual atoms that occupy hollow sites. This particular representation of the structure of the surface layer has been proposed[27] to reproduce the correct binding position of the adsorbed molecules on the Au(111) surface. (ii) A new generic atom type for the Au atom was introduced, with generic $\varepsilon_{\mathrm{AuAu}}$ and σ_{AuAu} LJ parameters to be used for calculating E_{LJ} for gold−water and gold−protein atom pairs. (iii) Specific LJ parameters for the interaction between Au and the unprotonated N atom in His and the S atoms in CysH/Met were optimized to introduce N−Au and S−Au chemical bonding, respectively. (iv) The ε_{ij} value of carbon atoms in π rings was fitted to reproduce the rather strong interaction between the π electrons of aromatic molecules and the metal surface observed experimentally (if the π ring is oriented parallel to the surface plane). (v) A shell type model describes polarization effects of the gold surface,[47] although the latter feature is not used in the calculations presented here. Details on the derivation of the GolP parameters and a comparison between the adsorption energies calculated with GolP and experimental results for different molecules (typical deviations of less than 5−10% or a few kJ/mol), can be found in ref 27.

The direct pairwise calculation of the E_{LJ} energy between all atoms of the protein and of the metal cluster is too expensive for the large biological molecules usually studied by BD methods. Therefore, a grid-based procedure was implemented in which the LJ interaction energy between the protein and a gold atom is saved on the nodes of a three-dimensional grid with the origin placed at the protein center. The grid size is chosen so that the long-range limit of the protein atom−Au interactions with a cutoff of ∼10 Å is inside the LJ grid. Then, the E_{LJ} interaction energy between the gold surface and a protein can be obtained by summation over all Au atoms of the gold cluster.

The balance between the repulsive and attractive parts of the LJ potentials arising from neighboring protein atoms is extremely important at small protein−surface distances. The binding energy is thus very sensitive to the grid spacing. Our test calculations of amino acid adsorption in a vacuum showed, for example, that a spacing of 0.2 Å may lead to an error in binding energy of up to about 3 kJ mol^{-1} compared to the binding energy of amino acids obtained directly by summation of the pairwise terms in eq 3. For comparison, a grid spacing of 0.5 Å results in an error in the binding energy of up to 12 kJ mol^{-1}. Therefore, a grid spacing of 0.2 Å has been used throughout the present study. Both the accuracy of the computed energy and the calculation speed depend on the number of gold layers employed. The optimal number of layers is three, since the energy correction due to adding a fourth layer is smaller than the uncertainty due to the grid discretization.

At short interaction distances (less than the sum of the atomic van der Waals radii in the OPLS force field), a constant positive energy of 100 kJ mol^{-1} was assigned to avoid very strong repulsion and therefore excessively high forces in BD simulations.

2.2.2. Protein−Metal Electrostatic Free Energy in an Aqueous Solution: U_{EP}. The interaction of a fixed set of partial point charges with a flat infinite uncharged metal surface is represented in classical electrostatics by the interaction between real charges q_i and their image charges, $q_i^{img} = -q_i$, placed symmetrically with respect to the metal surface plane. This approximation was shown to give good agreement with density functional calculations at a surface-charge distance of >2.5 Å.[48] Likewise, the electrostatic field of a fixed charge density in a nonuniform dielectric medium in the presence of the uncharged metal surface can be simulated by introducing an oppositely charged mirror image of the charge system instead of the metal surface. It is important that, to satisfy the boundary conditions (zero surface potential of the metal), electrostatic potentials of the protein and its opposite-charged image should exactly cancel each other at the surface plane. Therefore, not only the spatial distribution but also the dielectric surroundings of the real/image charges should be symmetrical with respect to the metal surface plane. Practically, in the implicit solvent model, a protein interacting with its image system consists of two charge distributions (one distribution for the real protein and one for its image), each immersed in low dielectric cavities surrounded by a high dielectric solvent and separated by a low dielectric cavity that surrounds the metal surface. The latter cavity is introduced since the centers of the surface layer of metal atoms (defining the metal surface plane) are separated from the solvent by the LJ radius for the metal−water interaction.

The image potential is defined as $\Phi^{im}(\vec{r}_i^{im}) \equiv -\Phi(\vec{r}_j^{p})$, where $\vec{r}_i^{im} \equiv (x_i^p, y_i^p, z_i^p + 2z_{CG})$ and $\vec{r}_j^{p} \equiv (x_i^p, y_i^p, -z_i^p - 2z_{CG})$ are vectors from the geometric centers of the image and real protein, respectively, and z_{CG} is the distance between the protein center and the metal surface as illustrated in Figure 1. Hence, we replace the protein−metal electrostatic interaction by a protein-image interaction with an additional low-dielectric cavity between the protein and the image as illustrated in Figure 1.

The electrostatic interaction free energy of two macromolecules (including solvent-related entropic effects only) can be calculated by numerical solution of the Poisson−Boltzmann equation. This however requires considerable computational resources and cannot be done at each time step of a BD simulation. Alternatively, the problem can be quite accurately solved by using the effective charge approximation for macromolecules (ECM) developed for protein−protein interactions.[49] Following this work, we describe the electrostatic interaction free energy between a protein and its image in the presence of the metal cavity as

$$U_{EP} = U_p/2 + U_{im}/2 + U_{p-c} + U_{im-c} \quad (4)$$

where U_p (U_{im}) corresponds to the energy of interaction of the protein (image) charges with the image (protein) electrostatic potential computed in the presence of both protein and image cavities as well as the metal cavity; U_{p-c} (U_{im-c}) describes perturbation of the protein (image) electrostatic potential by the low-dielectric cavity of the image (protein). The latter term decreases rapidly with the protein-image distance (i.e., with the distance from the metal surface) and will be referred to hereafter as the electrostatic desolvation energy.

The first and the second terms in eq 4 are equal, and so are the third and fourth terms. Thus,

$$U_{EP} = U_p + 2U_{p-c} \quad (4a)$$

For the real protein, the effective charges, q_i^{eff}, in a uniform high dielectric medium give the same electrostatic potential outside the protein surface as that computed for the real protein treated as a low dielectric cavity immersed in high dielectric solvent.[49] The electrostatic energy, U_p, can then be approximated by the interaction energy of the real protein effective charges q_i^{eff},[49] immersed in a uniform solvent medium, with the electrostatic potential of the protein image

$$U_p = \sum_i \Phi^{im}(\vec{r}_i^{im}) q_i^{eff} \text{ (where } \Phi^{im}(\vec{r}_i^{im}) \equiv -\Phi(\vec{r}_j^{p})) \quad (5)$$

The electrostatic potential, $\Phi(\vec{r}_j^{p})$, of a protein in water was calculated by numerically solving the linearized Poisson−Boltzmann equation using the UHBD (University of Houston Brownian Dynamics) program.[50] The relative dielectric constant of the protein was assigned as 4 and that of the solvent as 78, and the dielectric boundary was defined by the van der Waals radii of the protein atoms. The protein

atoms were assigned partial charges from the OPLS force field.[46] The electrostatic potential was computed on a three-dimensional grid centered on the geometric center of the protein. Since the electrostatic potential changes smoothly with $\vec{r}$, it does not require as accurate a representation as the LJ potential, and we have therefore used a grid with a spacing of 0.5 Å in the present calculations. The effective charges q_i^{eff} were positioned on selected atoms of the charged residues (the carboxylate oxygen atoms of Asp and Glu residues, as well as the amine nitrogen atoms of Lys, Arg, and protonated His residues), and their values were derived by fitting the protein electrostatic potential in a 3-Å-thick layer extending outward from the protein's accessible surface computed with a probe of radius 4 Å.[49,51]

The last term in eq 4a is the electrostatic desolvation term of the protein with effective charges q_i^{eff} due to presence of the image protein cavity and the metal surface cavity. This can be accounted for by the introduction of a positive energy term analogous to that proposed in ref 49 as

$$U_{\text{p-c}} = \sum_i (\Phi_{\text{ed}}^{\text{met}}(\vec{r}_i) + \Phi_{\text{ed}}^{\text{im}}(\vec{r}_i)) \times (q_i^{\text{eff}})^2 \qquad (6)$$

A general equation for the electrostatic desolvation potentials, $\Phi_{\text{ed}}(\vec{r})$ [$\Phi_{\text{ed}}^{\text{met}}(\vec{r})$ or $\Phi_{\text{ed}}^{\text{im}}(\vec{r})$], due to a set of spherical low dielectric cavities is given in the dipole approximation in ref 52 as

$$\Phi_{\text{ed}}(\vec{r}_i) = \alpha \frac{\varepsilon_s - \varepsilon_p}{\varepsilon_s(2\varepsilon_s + \varepsilon_p)} \sum_j (1 + k\vec{r}_{ij})^2 \exp(-2kr_{ij}) \frac{a_j^3}{r_{ij}^4} \qquad (7)$$

k is the Debye−Hückel parameter, ε_p is the protein dielectric constant, ε_s is the solvent dielectric constant, a_j is the van der Waals radius of the jth atom of the protein image (or atoms of the metal surface), and r_{ij} is the distance from the jth atom to the effective charge of the protein q_i^{eff}. The scaling factor α was estimated[52] for protein−protein association as $\alpha = 1.67$. Since $\Phi_{\text{ed}}^{\text{met}}(\vec{r}_i)$ is at least 2^4 times larger than $\Phi_{\text{ed}}^{\text{im}}(\vec{r}_i)$ (eq 7), we can omit the effect of the image cavity on the electrostatic field of the protein and keep only the metal cavity terms:

$$U_{\text{EP}}(\vec{r}) = \sum_i \Phi^{\text{im}}(\vec{r}_i^{\text{im}}) q_i^{\text{eff}} + 2 \sum_i \Phi_{\text{ed}}^{\text{met}}(\vec{r}_i) \times (q_i^{\text{eff}})^2 \qquad (8)$$

The electrostatic energy given by eq 8 has been derived for the case of nonoverlapping cavities of the protein and the metal surface. To complete this model, we have to consider the case in which the adsorbed molecule penetrates the first hydration layer of the surface, which in the context of the implicit solvent model means that the low-dielectric cavities of the protein and the metal merge. In general, this has two effects: (i) The change in Born solvation energy should be taken into account; this, however, rapidly vanishes with increasing adsorbate size[53] and can be neglected in the case of molecular adsorption (the case of ions will be discussed at the end of the present section). (ii) The metal-charge interaction energy must be scaled appropriately for the transition from high to low dielectric surroundings.

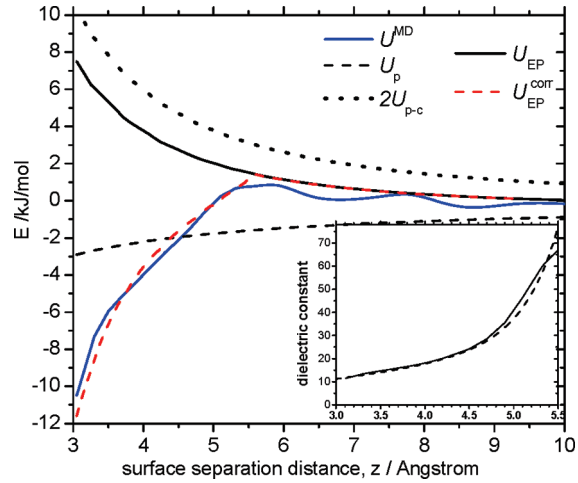

Figure 2. Total electrostatic energy for a test charge atom as a function of distance from the gold surface with explicit (U^{MD}) and implicit ($U_{\text{EP}}^{\text{corr}}$) water models ($U_p$, U_{EP}, and $U_{\text{p-c}}$ are separate contributions to the electrostatic energy, see text for details). Insert: Plot of effective dielectric constant derived from the image-charge potential computed from explicit water simulations (solid line) and approximated by an analytical function (dashed line).

Effect ii can be estimated from the electrostatic energy of an ion in the presence of the metal surface obtained in an MD model in which the solvent is treated explicitly. To this end, we have computed the image-charge energy, U^{MD}, of a test charge atom (with unit charge and $\sigma_{ii} = 2.87$ Å) as the difference in ion energy in explicit-water simulations with and without image-charge effects, see Figure 2. One can see in Figure 2 that, at surface separation distances smaller than $z \sim 5.5$ Å, the electrostatic ion-metal energy computed in the explicit water model, U^{MD}, is much lower than that obtained in the present implicit solvent approximation, U_{EP}. This z value can be considered as the approximate ion-surface distance at which the ion (or an effective charge in a molecule) and surface cavities start to merge. Indeed, this agrees with the Au−water and test charge−water LJ radii (~3 Å and ~2.5 Å, respectively).

The simplest way to account for this effect at small charge-surface distances in the ProMetCS model is to introduce a variable dielectric constant that increases as an effective charge moves away from the surface and reaches the value of $\varepsilon = \varepsilon_s$ when the cavities of the charge and the surface are separated and water molecules are able, at least partially, to screen the charge−metal interaction. Keeping the electrostatic desolvation energy $U_{\text{p-c}}$ unchanged, we fitted the dependence of the dielectric constant on the unit charge-surface separation distance, z, to reproduce the explicit-water electrostatic energy:

$$U_{\text{EP}}^{\text{corr}} \equiv \frac{-1}{2z(4\pi\varepsilon_0)\,\varepsilon(z)} + 2U_{\text{p-c}} \approx U^{\text{MD}} \qquad (9)$$

and therefore,

$$\varepsilon(z) = \frac{1}{2z(4\pi\varepsilon_0)(2U_{\text{p-c}} - U^{\text{MD}})}$$

The computed variable dielectric constant can be approximated by an analytical function $\varepsilon(z) = 4.0 + 0.8z^2 + \exp(z/0.385 - 10.4)$, where z is in Å, for $z < 5.5$ Å (see the insert in Figure 2).

In the case of a set of effective charges, the corrected electrostatic energy, U_{EP}^{corr}, can be directly applied to the diagonal terms, which correspond to the interaction of an effective charge i with its own image (for charge-surface distances of $z_i < 5.5$ Å):

$$U_{EP}^{corr} = U_{EP} + \sum_i \frac{(q_i^{eff})^2}{2z_i(4\pi\varepsilon_0)}\left(\frac{1}{\varepsilon_s} - \frac{1}{\varepsilon(z_i)}\right) \qquad (10)$$

This approximation is valid for the case of amino acids that are described by one effective charge in the ECM model,[49] but for a system of many effective charges, cross-terms that correspond to the interaction between a charge and the image of another charge should also be taken into account.

The minimum value of the relative dielectric constant is ~10 (see Figure 2), which is consistent with typical values used in modeling of the electrochemical interface.[54] This value can lead to an up to 4-times larger Coulomb energy for a monatomic ion in pure water.

2.2.3. Protein Nonpolar (Hydrophobic) Desolvation Energy. The free energy change of a protein due to its partial desolvation by the gold surface can be described by a nonpolar desolvation energy that is proportional to the solvent accessible surface area (SASA) of a protein and an energy coefficient (Φ_{pd}):[55]

$$U_{desolv}^{p} = \sum_m \Phi_{pd} SASA_m \qquad (11)$$

where the energy potential Φ_{pd} is computed on a three-dimensional grid and is defined as a function of the distance r from the van der Waals surface of a protein:[55]

$$\Phi_{pd}(r) = \beta c \begin{cases} 1 & \text{if} \quad r < a \\ \dfrac{b-r}{b-a} & \text{if} \quad a < r < b \\ 0 & \text{if} \quad r > b \end{cases}$$

The parameters a and b have been optimized[55] by using a standard method for SASA calculations (NACCESS) and are set to 3.1 Å and 4.35 Å, respectively; $c = 0.5$; the coefficient β was set to ~ -0.021 kJ mol^{-1} Å^{-2} in the present calculations. It should be noted that the regions of nonzero desolvation energy and LJ binding energy strongly overlap, and this may lead to the relatively smaller hydrophobic desolvation term being dominated by the larger LJ attraction.

2.2.4. Metal Desolvation Energy for Nonpolar Adsorption Sites. To understand the nature of the solvation effects arising from the partial replacement of the metal hydration shell by a biomolecule, we considered the properties of the water in the vicinity of the Au(111) surface that can be derived from MD simulations. We first computed the partial water density as a function of surface water separation distance from a simulation of bulk water in the presence of an Au(111) surface, see Figure 3. The hydration shell consists of two water layers (at 3 Å and 6 Å) with a high partial density of water molecules. The comparison of the density of oxygen and hydrogen inside the first and second layers is higher than that of hydrogen, which indicates a nonuniform orientation of the water molecules, in agreement with other studies.[38,40] We then computed the PMF for one water molecule as a function of the surface water separation distance, see Figure 4. From the PMF, the computed binding free energy for a water molecule is ~ -2.8 kJ mol^{-1} and ~ -0.6 kJ mol^{-1} for the first and second hydration layers, respectively. The bound water in the first hydration layer is separated by a free energy barrier of ~ -4.4 kJ mol^{-1} from the bulk water. The PMF shows that there will be an unfavorable positive energy change of the solvent-metal system when a water molecule is removed from the hydration shell to the bulk.

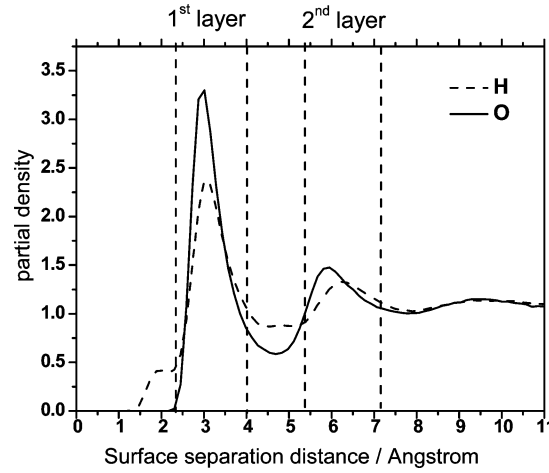

Figure 3. Dependence of the partial density of the water oxygen atoms (solid line) and hydrogen atoms (dashed line) on the distance from the gold surface computed from MD simulations of water in the presence of a gold surface. Densities are normalized to the bulk values; details of calculations are given in Appendix I.

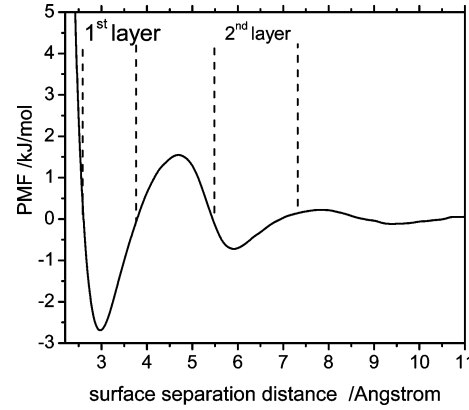

Figure 4. PMF of a water molecule as a function of the distance from the surface computed from MD simulations. Details of calculations are given in Appendix I.

The metal desolvation energy is the free energy change caused by the replacement of the hydration shell of the metal surface by the protein adsorption site. It is, therefore, reasonable to assume that the desolvation energy is proportional to the desolvated area of the metal so that we can use an expression similar to eq 11:

$$U^{m}_{\text{desolv}} = \sum_{i} \Phi_{\text{metd}} S^{\text{desolv}}_{i} \tag{12}$$

where the coefficient Φ_{metd} is a free energy change for desolvation of a unit surface area of the metal. A proper modeling of the metal desolvation requires Φ_{metd} to depend on the distance of the protein surface atom i from the atoms of the metal surface. At large separations, when the distance between a protein atom i and the metal surface is greater than the LJ cutoff value, $Z_{\max}$, Φ_{metd} must converge to zero. The summation in eq 12 must be carried out over the protein surface atoms, and S^{desolv}_{i} defines a desolvated area of the metal surface associated with the contacting protein atom i.

In the ProMetCS model, the desolvation energy describing replacement by a protein atom i of the first ($z_i < Z_{\text{adw}}$) and the second and higher ($z_i > Z_{\text{adw}}$) hydration layers is given by

$$\Phi_{\text{metd}} = \begin{cases} \Phi^{0}_{\text{metd}} & z_i \le Z_{\text{adw}} \\ \Phi^{0}_{\text{metd}} \exp(-(z_i - Z_{\text{adw}})/\gamma)) & Z_{\text{adw}} < z_i < Z_{\max} \\ 0 & z_i > Z_{\max} \end{cases} \tag{13}$$

where z_i is the distance between the center of the protein surface atom i and the metal surface, Φ^{0}_{metd} is the desolvation energy per unit area of the first hydration layer, γ describes the decrease in magnitude of the desolvation energy when the second and higher hydration layers are replaced, Z_{adw} corresponds to the position of the first hydration layer as defined above (~3 Å) plus the average LJ radius for the protein−metal atom interaction, which gives $Z_{\text{adw}} \sim 5$ Å, and $Z_{\max} \sim 10$ Å is the cutoff for computing the desolvation term. Using the binding free energies per water molecule derived from the PMF in Figure 4, and assuming that the surface area occupied by one water molecule is ~9 Å^2, we estimate $\Phi_{\text{metd}} \equiv \Phi^{0}_{\text{metd}} \sim 0.31$ kJ mol^{-1} Å^{-2} and $\Phi_{\text{metd}} \sim 0.07$ kJ mol^{-1} Å^{-2} for the first and the second hydration layers, respectively, which leads to an assignment of $\gamma \sim 1.51$ Å.

It should be noted that the desolvation energy U^{m}_{desolv} of eq 12 represents only the part of the free energy change of the metal hydration shell due to replacement of parts of the hydration shell by a noninteracting cavity. Electrostatic effects caused by the interaction of the charges at the adsorption site with oriented water dipoles on the metal surface (see Appendix II) are neglected here. Hence, the value of Φ^{0}_{metd} estimated from the water adsorption energy is only a first approximation that may need further correction.

In order to calculate the desolvation area due to binding of a protein, we placed a two-dimensional grid on the surface plane, centered on the protein. Then, the positions of all protein atom−metal contacts with $z_i < Z_{\max}$ were stored on the grid, and the area defined by the distance around the contact points R_{adw} (defined below) was considered as the desolvation area (illustrated in Figure 5). The total contact areas for atoms with $z_i < Z_{\text{adw}}$ and with $Z_{\text{adw}} < z_i < Z_{\max}$ were calculated separately (they are shown in Figure 5 by the bold solid and dashed lines, respectively). These areas were then multiplied by the corresponding energy coefficients given by eq 13.

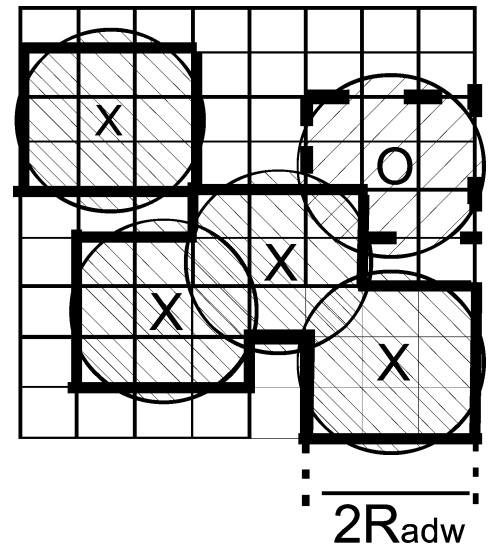

Figure 5. Illustration of the method employed for the calculation of the metal surface area in which water molecules are replaced by the adsorption site of the protein. The crosses and zeros show the positions of the centers of the protein atoms, with $z < Z_{\text{adw}}$ and $Z_{\text{adw}} < z < Z_{\max}$, respectively. The hatched circles with radius R_{adw} show the area each atom is assumed to desolvate. The computed desolvation area is shown by bold lines, the solid and dashed lines corresponding to water desorption from the first and second hydration layers, respectively. See the text for details.

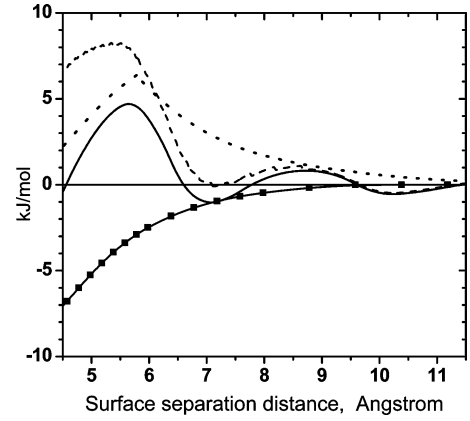

Figure 6. PMF obtained from MD simulations for the test atom (solid line), corresponding LJ potential (squares), and their difference (dashed lines) associated with the desolvation energy. Dotted line, PMF energy computed using the present model (includes both LJ and metal desolvation energies).

The value of R_{adw} was estimated by considering the desolvation energy, S^{desolv}, of a single test atom with "iodine-like" force-field parameters ($\sigma_{ii} = 5.4$ Å, $\varepsilon_{ii} = 0.293$ kJ mol^{-1}) that mimics a small nonpolar functional group of a protein. The PMF of the test atom obtained from MD simulations using a harmonic restraint potential applied along the z axis (the x and y coordinates were fixed during the simulations) is shown in Figure 6, along with the corresponding LJ potential. Since the translational entropy change along the PMF is zero for the present case, the difference between the PMF and LJ energies (dashed line in Figure 6) corresponds to the metal desolvation energy. It shows maxima at the first and second hydration layers at surface

separation distances of ~5.5 Å and ~8.5 Å, respectively. From the magnitude of the energy maxima, we estimate the desolvation energy change associated with partial replacement of the first hydration layer by an adsorbed atom as $U^m_{\text{desolv}} = 8.4$ kJ mol^{-1}. With $\Phi^0_{\text{md}} = 0.31$ kJ mol^{-1} Å^2, $S_i^{\text{desolv}} \sim 27$ Å^2, which can be described by an effective desolvation radius, R_{adw}, of ~3 Å. The total adsorption energy for the test atom computed as a function of the separation distance with the ProMetCS model with the parameters derived above is shown by the dotted line in Figure 6. The energy function given by eq 13 is by definition not able to reproduce the energy fluctuation at $z_i > Z_{\text{adw}}$, but in the case of a protein, the contribution of this effect is expected to be relatively small. The value of $R_{\text{adw}} = 3$ Å was used throughout all the calculations and appeared to be a good first approximation, as will be shown below.

2.3. Calculation of the Adsorption Free Energy and Potential of Mean Force. We consider an adsorbate as a rigid molecule moving relative to the solid surface. The geometry of the simulation box is the same as described above and shown in Figure 1. An adsorbate energy, defined by eq 1, is generally a six-dimensional function of the protein position and orientation. Three translational degrees of freedom define the position of the molecular center of geometry, x_{CG}, y_{CG}, and z_{CG}, where $\vec{r}_{\text{CG}} = (x_{\text{CG}}, y_{\text{CG}}, z_{\text{CG}})$, and the three rotational coordinates, $\Omega = (\Omega_1, \Omega_2, \Omega_3)$, are represented by Euler angles of the coordinate frame centered at the protein.

The solid surface is usually characterized by a periodic structure, and one can, therefore, expect a periodic variation of interaction energy as the protein position is shifted in the *xy* plane. Without any loss of generality, the molecule motion in the *xy* plane can, therefore, be considered in the area of $\Delta S = \Delta x_{\text{CG}} \Delta y_{\text{CG}}$, where Δx_{CG} and Δy_{CG} define a period of energy variation along the corresponding coordinate. The unit volume of configurational space of the protein−surface system is defined as $\mathrm{d}S\, \mathrm{d}\Omega\, \mathrm{d}z$ ($\mathrm{d}S = \mathrm{d}x_{\text{CG}}\, \mathrm{d}y_{\text{CG}}$, $\mathrm{d}\Omega = \sin \Omega_1\, \mathrm{d}\Omega_1\, \mathrm{d}\Omega_2\, \mathrm{d}\Omega_3$), and the total simulation volume of the configurational space is $8\pi^2 \Delta S b$.

The free energy change upon protein adsorption is then given by[56]

$$\Delta G = -k_{\text{B}}T \ln\left[\frac{Q_{\text{b}}}{Q_{\text{f}}}\right] = -k_{\text{B}}T \ln\left[\frac{\int_{\text{b}} \mathrm{d}z \int_{\Delta S,\Omega} \mathrm{d}\Omega\, \mathrm{d}S \exp(-U(\vec{r}_{\text{CG}}, \Omega, S)/k_{\text{B}}T)}{b 8\pi^2 \Delta S}\right] \tag{14}$$

where Q_{b} and Q_{f} denote configurational partition functions of an adsorbate in the bound and free states per unit volume, $S = (x,y)$, and

$$Q_{\text{b}} = \frac{\int_{\text{bound}} \mathrm{d}z \int_{\Delta S,\Omega} \mathrm{d}\Omega\, \mathrm{d}S \exp(-U(\vec{r}_{\text{CG}}, \Omega, S)/k_{\text{B}}T)}{V_{\text{b}}} \tag{15}$$

The value $Q_{\text{f}} = 8\pi^2$ represents a uniform distribution of an unbound protein over configurational space, and $V_{\text{b}} = \Delta S b$ is the simulation volume.

Direct calculation of the complete 6-dimensional free energy landscape is difficult, and we have therefore used the system symmetry to reduce the dimensions of the energy matrix. First, due to the periodicity of the interaction potential along the x_{CG} and y_{CG} coordinates, only a small area, ΔS, must be explored. A period of the interaction potential is about the dimension of the Au metal cell. In fact, preliminary calculations showed that the greatest variations in potential occur within an area of 6 × 6 Å with a grid spacing of 0.5 Å; i.e., 13 ×13 grid nodes should be computed for the x_{GC} and y_{GC} coordinates. Variations in potential in the *xy* plane as well as with respect to rotation around *z* (Ω_3 angle) arise only from the short-range energy terms (i.e., LJ and desolvation energy terms) and can therefore be neglected if the smallest separation between protein surface atoms and the metal surface, z_{min}, is larger than the LJ cutoff, $Z_{\text{max}} \sim 10$ Å. Thus, at large distances, only the electrostatic component is important, and only three coordinates, Ω_1, Ω_2, and z_{GC}, must be explored. Moreover, since the electrostatic potential is quite smooth, the grid spacing over z_{GC} can be notably increased at $z_{\text{min}} > Z_{\text{max}}$. After some test calculations, we chose a grid spacing $\mathrm{d}\Omega_1 = \mathrm{d}\Omega_2 = 3°$, $\mathrm{d}\Omega_3 = 6°$, and $\mathrm{d}z_{\text{GC}} = 0.2$ Å at $z_{\text{min}} < Z_{\text{max}}$, and $\mathrm{d}\Omega_1 = \mathrm{d}\Omega_2 = 6°$, $\mathrm{d}\Omega_3 = 12°$, $\mathrm{d}z_{\text{CG}} = 2$ Å at $z_{\text{min}} > Z_{\text{max}}$.

Computation of the free energy change upon binding using standard molecular dynamics simulations is not feasible since it requires very extensive sampling to reach and cross high-energy regions of the underlying energy landscape. To overcome this problem, enhanced sampling techniques, such as those based on the umbrella-sampling concept,[57,58] can be used. To explore a reaction coordinate *z*, a series of simulations can be performed with a biasing harmonic restraint potential defined at each point of interest, z^0_{CG}, along the reaction coordinate: $V(z_{\text{CG}} - z^0_{\text{CG}}) = -1/2k(z_{\text{CG}} - z^0_{\text{CG}})^2$.[58] The biased energy distribution function is given by $\exp(-(U(\vec{r}_{\text{CG}}, S, \Omega) + V(z_{\text{CG}} - z^0_{\text{CG}}))/kT)$, and, for a very sharp harmonic potential, the energy distribution function can be approximately described as

$$\exp(-(U(\vec{r}_{\text{CG}}, S, \Omega) + V(z_{\text{CG}} - z^0_{\text{CG}}))/kT) \approx \delta(z_{\text{CG}} - z^0_{\text{CG}}) \exp(-U(\vec{r}^0_{\text{CG}}, S, \Omega))/kT)$$

where $\delta(z_{\text{CG}} - z_0)$ is the Dirac delta function and $\vec{r}^0_{\text{CG}} = (x_{\text{CG}}, y_{\text{CG}}, z^0_{\text{CG}})$. In this case, we are concerned with a local function at fixed $z_{\text{CG}}{}^0$ that describes the Boltzmann distribution over the adsorbate positions in the $x_{\text{CG}}y_{\text{CG}}$ plane and over the adsorbate orientation. Instead of an adsorption free energy given by eq 14, we have a PMF along the reaction coordinate, z_{GC}, with

$$G_{\text{PMF}}(z^0_{\text{CG}}) = -k_{\text{B}}T \ln\left[\frac{\int_{\Delta S\Omega} \mathrm{d}\Omega\, \mathrm{d}S \exp(-U(\vec{r}^0_{\text{CG}}, \Omega, S)/k_{\text{B}}T)}{8\pi^2 \Delta S}\right] \tag{16}$$

It is important to note that the $G_{\text{PMF}}(z_{\text{CG}})$ given by eq 16 includes the same kinds of entropy contributions as the MD simulations and can, therefore, be directly compared with the MD results.

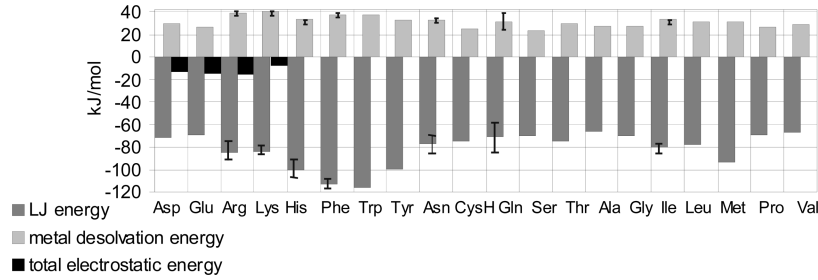

Figure 7. Contribution of the LJ, metal desolvation, and electrostatic (U_{EP}^{corr}) terms to the binding energy of capped amino acids on gold as calculated with the ProMetCS energy function. Error bars show energy deviation for different binding conformations used in simulations.

3. Results and Discussion: Testing of the Model for Adsorption of Capped Amino Acids on the Au Surface

To evaluate the accuracy of the energy model described, we computed the adsorption free energies and the PMFs of capped amino acids and compared the results with those obtained in MD simulations reported recently.[28,29] The main aim of this comparison was the testing of the proposed implicit solvent model against results with an explicit representation of water molecules. However, the solvent representation is obviously not the only difference between the ProMetCS energy function and that used in the MD simulations. To minimize the differences in physical characteristics of the amino acid−gold−water system employed in the two models, we used the same structure of the gold cluster and the same force-field parameters for the LJ energy as used by Hoefling et al.[28,29] Furthermore, in both models, an image-charge approximation was employed for calculation of the electrostatic effects. Finally, we used the most populated binding conformation of each capped amino acid obtained in MD simulations[28,29] in the present simulations. If several conformations with comparable populations were reported, we carried out simulations for all of them separately. However, we did not take into account the change in internal energy of the molecules upon conformational transition during the adsorption process, and this may cause some uncertainty in binding energy as will be discussed below in more detail.

Before presenting the results of the PMF simulations, let us consider the relative contributions of the energy terms of eq 1 to the binding energy of the amino acids. The largest contribution to the binding energy for almost all the amino acids arises from the LJ term, see Figure 7. As can be expected, the LJ energy increases with the number of atoms contacting the surface and, therefore, tends to increase with the size of the amino acid side chain. Due to the empirical design of the GolP force field parameters used in the present study, the binding to gold of Cys, Met, and His is favored if sulfur or nitrogen, respectively, comes close to the surface. Similarly, molecules with π rings (His, Phe, Trp, Tyr) are rather strongly bound to gold if their rings are parallel to the plane of the surface. Indeed, the absolute value of the LJ term shown in Figure 7 demonstrates the largest magnitudes for His, Met, Phe, Tyr, and Trp. In His, we found that binding through the π ring is stronger than attraction via an unprotonated nitrogen atom, and in our calculations, the conformation with the ring parallel to the plane of the surface is more preferable than the tilted one.

The image-charge interaction is quite weak because of the charge-image distances (>6 Å) and the high dielectric constant aqueous medium between them. Indeed, the image-charge energy (first term in eq 8, U_p) is ~ -1.5 kJ mol^{-1} for all charged amino acids. Moreover, as an effective charge approaches the metal surface, induced solvent polarization around the low-dielectric cavities makes the electrostatic interaction effectively repulsive. This effect is described by the positive electrostatic desolvation penalty ($2U_{p-c} \sim +5-7$ kJ mol^{-1} at an ionic strength of 150 mM used in the MD simulations). In fact, the total electrostatic energy becomes negative only when an effective charge penetrates the hydration shell of the metal and its field is not screened by the water molecules any more. This effect, simulated by the variable dielectric constant, leads to an electrostatic energy of about -7 to -14 kJ mol^{-1} for charged residues, which is, however, still notably smaller than the $|E_{LJ}|$ binding energy of up to ca. 115 kJ mol^{-1}.

Whereas the electrostatic contribution to binding to a neutral gold surface is small for capped amino acids, as is the favorable hydrophobic protein desolvation energy ($|U_{desolv}^{p}| < 3$ kJ mol^{-1}), the positive metal desolvation penalty varies from $+20$ kJ mol^{-1} to $+40$ kJ mol^{-1} and provides the largest compensation to the LJ term, see Figure 7. Since, U_{desolv}^{m} is proportional to the capped amino acid−metal contact area, the larger residues are in general characterized by a larger desolvation penalty as well as larger LJ binding energies. From Figure 7, one can also see that residues with long side chains, such as Arg and Lys, have a larger desolvation penalty than more compact residues. On the other hand, comparing all amino acids, the difference in the U_{desolv}^{m} value does not exceed 15 kJ mol^{-1}, while the LJ energy differs by up to $\sim$50 kJ mol^{-1}.

Finally, the binding energy is additionally compensated by the loss in translational and rotational entropy of the molecule upon binding to the surface. The entropy contribution has quite a small dependence on the amino acid type since all the capped amino acids have a well-defined binding position that corresponds to a rather sharp energy minimum. The entropic part due to restriction of rotation and of translation in the *xy* plane (which is included in the PMF) is about 25 kJ mol^{-1}, whereas the entropy difference due to translation along the *z* coordinate is $\sim$10 kJ mol^{-1}.

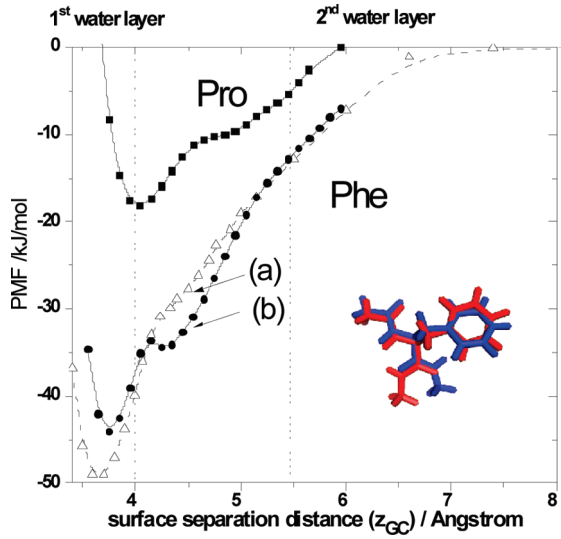

Figure 8. Representative PMF profiles computed using the ProMetCS model for two capped amino acids shown as a function of surface the separation distance: squares, Pro; triangles, circles, Phe. For Phe, PMFs computed for two slightly different conformations are shown: the aromatic ring is in the backbone plane (a, red conformation) and slightly tilted (b, blue conformation). Phe conformations are shown in projection onto the Au surface plane.

Representative PMF profiles for weakly (Pro) and strongly (Phe) bound residues are shown in Figure 8. The shape of the PMF, and the value of its global minimum depend on the conformation of the molecule used in the simulations. For example, the Phe conformation with the aromatic ring and backbone oriented in the same plane is more strongly bound and has only one minimum, whereas tilting the aromatic ring with respect to the backbone plane leads to two minima in the PMF (at ~3.7 Å and ~4.4 Å, see Figure 8), corresponding to the orientation of either the side chain or the backbone in the surface plane, respectively.

From the above analysis, we conclude that the relative binding strength of the amino acids in the present model is mainly driven by the LJ energy term. Since the LJ binding energy is very sensitive to the positions of the interacting atoms, conformational effects can be very important in the adsorption energy calculations. However, with the rigid-body approximation, the conformation is not adjusted at each simulation step, and therefore, changes in the internal energy of adsorbed molecules are not included in the present simulations. Therefore, to account for the existence of multiple conformations and minimize the uncertainty in the computed energies due to neglecting the change in internal molecular energy upon binding, calculations were carried out for some of the capped amino acids for several of the most populated binding conformations obtained in the MD simulations.[28] For most of the residues, there was only one dominant binding conformation in the MD simulations. For Asn, Arg, Cys, Gln, Glu, Leu, Lys, and Tyr, however, there were two bound conformations with similar populations, and for Ile, there were at least three conformations. The variation in binding energies obtained in the ProMetCS model for the different conformations is less than within ~5 kJ mol^{-1} for most of these amino acids, except for Gln, Ile, and Cys, whose

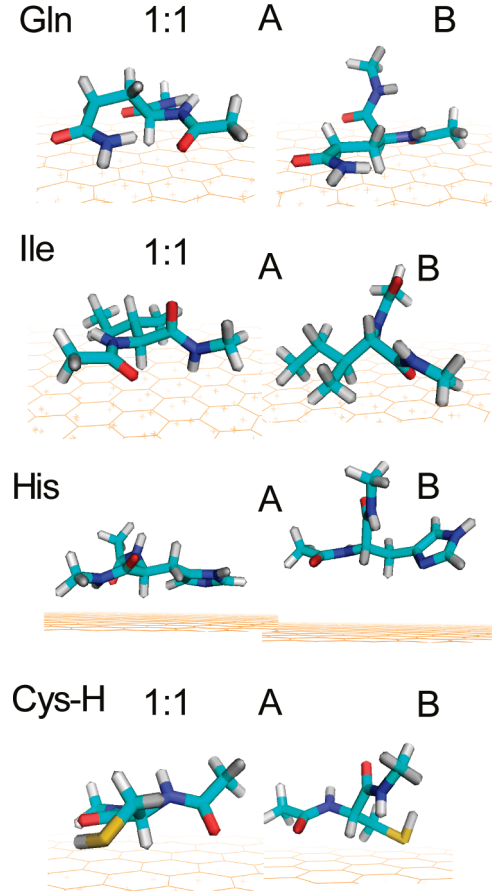

Figure 9. The most populated binding conformations of capped amino acids[28] for which significant dependence of computed PMF binding energy on conformation was observed, shown with their relative populations in the MD simulations. The corresponding PMF binding energies computed with the ProMetCS model are as follows: Gln, −40 (A) and −27 (B) kJ mol^{-1}; Ile, −24.3(A), −16.3 (B) kJ mol^{-1}; His, −48 (A), −31.9 (B) kJ mol^{-1}, where configurations A and B correspond to HIE and HID, respectively; CysH, −43 (A), −33(B) kJ mol^{-1}.

binding energy variation reaches ~10−15 kJ mol^{-1}. The most populated binding conformations for the latter residues are shown in Figure 9 along with their relative populations; the corresponding computed PMF binding energies are given in the figure caption. For all of these residues, the most strongly bound conformation has a nearly "flat" geometry (denoted as A in Figure 9) with the side chain as well as part of the backbone oriented parallel to the plane of the surface so that the LJ energy is optimized for the most atoms. In Figure 9, two binding conformations of His, "flat" and "tilted", which were observed in MD simulations[28] for two His forms corresponding to protonation of different nitrogen atoms in the aromatic ring (HIE, HID), are also shown. These have a binding energy difference of ~16 kJ mol^{-1} in the present calculations with the ProMetCS model, but almost equal binding free energies were computed from the MD simulations.[29] Here, the energy difference may be caused by underestimation of the desolvation penalty of the aromatic ring if it is placed in the surface plane since, as noted above, the U^{m}_{desolv} value is relatively small for aromatic residues.

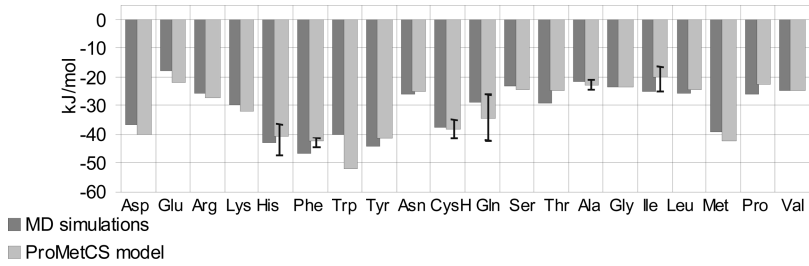

Figure 10. PMF binding free energies of the capped amino acids on the gold surface obtained using the ProMetCS model and MD calculations[29] as calculated with the ProMetCS energy function. Error bars show energy deviation for different binding conformations used in simulations.

Figure 10 shows a comparison of the PMF binding energies (the minimum of the PMF along the z coordinate) computed from the MD simulations[29] and with the ProMetCS model. For the residues mentioned above, characterized by several binding conformations in MD simulations that have notably different binding energies in ProMetCS, the PMF energies for the different conformations were averaged with equal weights. With the exception of Trp, the deviation of the PMF binding energies computed with the ProMetCS model from those from MD simulations does not exceed 5 kJ mol^{-1}. The binding energy of Trp is overestimated by $\sim$13 kJ mol^{-1}, which may be due to two reasons: (i) underestimation of the metal desolvation energy for aromatic residues, which was discussed above and might be especially pronounced in the case of Trp (the notable overestimation of the binding energy for conformation A of His is consistent with this suggestion, see Figure 9); (ii) a conformational energy change upon binding that is not taken into account in these calculations.

Taken into account the uncertainties in the present calculations, we can select capped amino acids with adsorption energies below -40 kJ mol^{-1} and above -25 kJ mol^{-1} and assign them to groups of strongly and weakly bound amino acids, respectively. Thus, His, Met, Phe, Trp, and Tyr belong to the group of strong binders, whereas Ala, Glu, Gly, Ile, Leu, Pro, Ser, and Val can be described as weak binders. The list of "strong binders" agrees with the experimental study of Peelle et al.,[5] in which notable binding was observed only for homopeptides of Cys, His, Met, and Trp. Furthermore, high affinity to the gold lattice has also been suggested for Trp and Tyr by Hnilova et al.[9] However, Phe was not mentioned among the amino acids with high affinity to gold reported in these experimental studies.[5,9]

In general, some overestimation of computed binding energy relative to that observed experimentally might be expected because, in particular, there should be some conformational restrictions on the amino acids in the peptides studied in experiments (i.e., the optimal binding conformation of an amino acid on the surface may be greatly unfavorable in the peptide). Furthermore, the binding to gold of the capping residues used in the calculations may additionally contribute to the computed affinity, leading to some overestimation of binding strength, especially for weakly bound residues. For example, the adsorption free energy of L-phenylalanine derived from electrochemical measurements[7] was characterized as typical for weak chemisorption of small aromatic molecules (from -18 to -37 kJ mol^{-1}, where the larger value is associated with electrostatic binding of the carboxylic group to a positively charged electrode). Considering that, in the present simulations, about 20$-$25 kJ mol^{-1} of the adsorption energy of the capped Phe molecule come from the capping residues (see adsorption geometry of Phe shown in Figure 8), the binding energy of the Phe residue can be estimated as $\sim -25-30$ kJ mol^{-1}, which is in the range of experimental values.

4. Summary and Future Directions

In the present paper, we propose an approximation for the calculation of the binding free energy of biomolecules on an atomically flat uncharged Au(111) surface in a continuum aqueous solvent. The interfacial interaction energy is based on an atomistic representation of short-range interactions (van der Waals, weak charge transfer, π orbital interactions) that are approximated by a set of Lennard-Jones potentials, electrostatic interactions described by the image charge method combining with the effective charge approximation, and adsorbate desolvation and metal desolvation free energies. The latter term simulates the solvation free energy change due to the replacement of part of the gold hydration shell by the uncharged binding region of an adsorbate and has been parametrized by using the results of MD simulations of water molecules on gold. MD simulations were also the basis for parametrizing a model of the desolvation effects based on the electrostatic energy. The case when the adsorption site of the biomolecule is charged and interacts with the induced electrostatic field of the oriented water dipoles on the gold surface was also considered. When parametrized using the PMFs for surface binding of negatively and positively charged ions obtained from MD simulations, this effect was found to generally lead to slightly stronger binding of positively charged adsorbates than negatively charged ones (see Appendix II).

The proposed energy model, ProMetCS, has been verified against the recently reported PMFs of capped amino acids obtained from MD simulations.[29] We computed the binding energy of 1$-$3 of the most populated binding conformations observed in the MD simulations for each amino acid.[28,29] When averaged over these conformations, the computed PMF minimum values (i.e., PMF binding energies) reproduce the results of MD simulations with an error of less than 5 kJ mol^{-1} for all residues except Trp. The trends in amino acid

binding to gold are mostly in agreement with available experimental observations of the binding of homopeptides to gold despite the different conditions of the experiments.[5,7,9]

Analysis of the computed binding energies, in particular in comparison with experimental data, gives strong evidence that short-range van der Waals interactions (described by LJ potentials) are a driving force for adsorption of amino acids to a neutral metal surface. The change of the solvation free energy upon adsorption species is positive due to unfavorable distortion of the structure of the water layer on the gold surface. The balance of the short-range LJ attraction and the surface desolvation penalty makes the adsorption energy very sensitive to conformational variations of the adsorbed species and the orientation of the molecule on the gold surface. Therefore, it is advisible to explore a range of adsorbate conformations that are energetically accessible in aqueous solution.

As can be expected, the image-charge electrostatic effects on amino acid−gold interactions are quite small in comparison with the LJ term and the metal desolvation penalty, except in cases where a charged residue penetrates the hydration shell of the metal surface. On the other hand, in adsorption kinetics of large molecules, the electrostatic effects may gain more importance due to their long-range character.

The next step in validation of the ProMetCS model will be to apply it to a set of proteins and compare it with experimental adsorption data on the relative binding properties. Furthermore, due to the time-saving grid-based technique employed in the present model, it can be extended to the simulation of coadsorption and adsorption kinetics.

Acknowledgment. We gratefully acknowledge the support of the European Union (FP6 NEST project no. 028331- Prosurf) and the Klaus Tschira Foundation. We thank Razif Gabdoulline, Michael Martinez, Stefan Richter, Bingding Huang, and Mykhaylo Berynskyy for their assistance with various aspects of this work.

Appendix I. MD Simulations with Explicit Water Molecules

Three MD simulations with explicit water have been performed for this work:

(i) MD simulation of the water−Au(111) interface.

(ii) Calculation of the PMF of "fluorine-like" ions, i.e., an ion/atom with the LJ parameters assigned in the OPLS/AA force field to F^-, but with a +1, 0, and −1 e charge.

(iii) Calculation of the PMF of an "iodine-like" neutral atom, i.e., a neutral atom with the OPLS/AA[46] LJ parameters corresponding to those for I^-.

All these calculations were performed with the GROMACS (version 3.3.3 and 4.0.1) software.[59] The simple point charge, SPC, model was used for water (with rigid internal geometry constrained by the RATTLE algorithm), while the force field used for the water−gold, ion−gold, and atom−gold interactions is GolP.[27] The Au surface was simulated by a 5-layer gold slab, using a $7 \times 4\sqrt{3}$ supercell. 3D periodic boundary conditions were used. A second Au slab was placed at ∼3.5 nm from the first in the direction perpendicular to the surface (z), to confine water in a fraction of the periodic box along z (10 nm). In this way, possible spurious effects due to fictitious periodicity along z were minimized. The interslab space is large enough to have a ∼1-nm-thick region of water behaving like bulk SPC water in the middle of the slab (as verified by density profile and oxygen−oxygen correlation functions). The precise value of the interslab space was adjusted for each simulation to yield the bulk density of SPC water at 1 bar of pressure and 300 K at the center of the water layer.

The PME electrostatic model was employed in all the simulations, using GROMACS defaults for the PME parameters. For neutral systems, we performed some tests employing the Yeh and Berkowitz[60] electrostatic corrections proposed for 2D periodic systems treated with 3D periodicity. No significant variation in the reported result was found. For charged systems, no counterions were inserted to neutralize the simulation box to avoid sampling issues.[61] All the simulations were performed in the NVT ensemble, with $T = 300$ K. LJ interactions were cut off at 1.0 nm.

For simulation i, an initial equilibration of 100 ps was followed by a 5 ns production run. The density profiles in Figure 3 were obtained from the resulting trajectory. The PMF of water in Figure 4 was obtained as

$$\mathrm{PMF}(z) = -RT \ln\left(\frac{d(z)}{d_{\mathrm{bulk}}}\right)$$

where $d(z)$ is the water density in the slab centered at z and d_{bulk} is the bulk density.

PMF calculations ii and iii were performed by integration of the average force along the ion-surface separation coordinate,[62] using either umbrella-biased simulations, also called umbrella integration[63] (calculation ii), or a constraint-biased simulation, with a LINCS constraint.[64] In both cases, an initial simulation was performed in which the ion/atom was pulled through the box, along the direction perpendicular to the surface, in 1 ns. From this simulation, 30 snapshots corresponding to 30 different ion-surface distances ranging from 0.25 to 1.2 nm were extracted. From each of these snapshots, a 5-ns-long simulation was started, keeping the ion/atom at the initial distance by using a tight harmonic restraint for ii or a constraint for iii. The thermodynamic restraint/constraint forces were collected during the last 3 ns of the dynamics and averaged to get the opposite of the PMF derivative with respect to the ion-surface distance. By numerically integrating such PMF derivatives, the PMF profiles in Figures 6 and 11 were obtained.

The ability of the GolP force field to reproduce experimental adsorption energies on gold for small molecules has been verified in ref 27, and the soundness of the calculated adsorption free energies of amino acids in solution is shown in ref 29. As a further test of the force field underlying ProMetCS, we calculated the central quantity to characterize the liquid water−gold interaction, i.e., the wetting coefficient k as defined by the relation $k = (\gamma_{sv} - \gamma_{sl})/\gamma_{lv}$ where γ_{sv}, γ_{sl}, and γ_{lv} are the solid−vapor, solid−liquid, and liquid−vapor interface tensions, respectively.[65] The difference $\gamma_{sv} - \gamma_{sl}$ was calculated from the 5 ns simulation described above in two ways: by the virial-based expression[65,66] as implemented in GROMACS 4.0.1 and by the energy-based method proposed in ref 20, using the entropic term correction

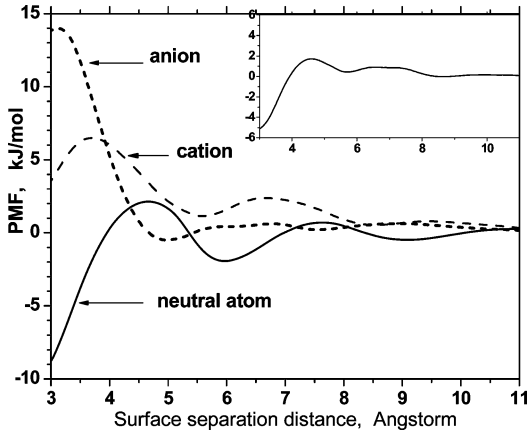

Figure 11. PMF of a test neutral atom (solid curve) and test positively and negatively charged ions (dashed and dotted curves, respectively) as a function of the surface separation distance. Insert depicts half of the difference between the PMF of a cation and of an anion.

proposed there. For the latter calculation, separate simulations of the gold slabs and the water slab were needed, and we performed simulations of 5 ns for each. In both cases, k was then calculated by using the value for γ_{lv} obtained by the virial method on the 5 ns water slab simulation. The virial-based expression yielded $k = 0.95 \pm 0.1$, while the energy-based expression yielded $k = 1.35 \pm 0.03$. For polycrystalline gold, it is known that $k \geq 1$ (i.e., the water contact angle $= 0°$), and for the Au(111) surface, a value close to or higher than 1 is also expected.[43] Therefore, the calculated k values are compatible with the experimental results. This discussion should not be considered as a detailed study of the water−gold surface tension obtained with GolP, which would require tests with respect to the cell size, the duration of the simulation, and the effects of the LJ cutoff. While such a detailed treatment is outside the scope of this article, it remains that the approximate k value computed here supports the use of GolP results in ProMetCS.

Appendix II. Electrostatic Interaction of an Ion with an Interfacial Water Potential

The electrostatic energy terms described above are derived for a uniform CS and do not take into account the effect related to the ordered water layer that directly contacts the metal surface. To estimate the contribution of this effect to the surface-binding energy of an ion, we first considered adsorption of test ions onto the metal surface. Computed PMFs for the positively and negatively charged test fluorine-like ion s, as well as a corresponding neutral atom, are shown in Figure 11.

The PMF function of an ion can be decomposed into four separate energy terms: (i) the LJ and the image-charge electrostatic interaction energies between the ion and the metal surface; (ii) the positive Born solvation energy given by $q/(8\pi\varepsilon_0 a)(1/\varepsilon_S - 1/\varepsilon_I)$[53] in the case of a charged atom of radius a that is transferred from a high dielectric ε_s to a low dielectric medium with dielectric constant ε_I; (iii) the free energy change of the solvent arising from distortion of the hydration shell of the metal (discussed above); and (iv) the interaction energy of the ion with the electrostatic field of the interfacial water.

Only the last term depends on the sign of the ion's charge and, therefore, can be computed as half of the difference between the PMF of the positively and negatively charged ions plotted in Figure 11. As expected, the resultant function (see insertion in Figure 11) shows fluctuations that roughly correlate with the variation of the oxygen partial density, i.e., with the negative partial charge variation within the hydration shell of the metal surface. One can also see from this plot, that term iv is relatively small (less than ~5 kJ mol^{-1}) and attractive for positively charged ions that are localized at an ion-surface distance of 3−4 Å (i.e., when the ion is inserted into the first hydration layer). On the other hand, the electrostatic field of the surface water layer is preferentially attractive for an anion when it is placed slightly beyond the first hydration layer, at 4−5 Å, which corresponds to the maximum of the hydrogen partial density.

The Born solvation energy is dominant at small distances ($z < 4$ Å) for ions but should be negligible for molecules. A charged fragment of a protein adsorption site would be surrounded by neighboring neutral atoms of the protein. This would mean that the electrostatic effect caused by the hydration shell would be less pronounced than for a bare ion because the charge-water distance would be too large to make the magnitude of the effect significant. Thus, the desolvation effect may be represented solely by the metal desolvation term iii due to the distortion of the hydration shell of the metal. Taking into account all these uncertainties and a modest contribution to the free binding energy, we did not implement the term accounting for this effect in the free energy calculations.

References

(1) Slojkowska, R.; Palys, B.; Jurkiewicz-Herbich, M. *Electrochem. Acta* **2004**, *49*, 4109–4118. Prado, C.; Prieto, F.; Rueda, M.; Feliu, J.; Aldaz, A. *Electrochim. Acta* **2007**, *52*, 3168–3180.

(2) Brown, S. *Nat. Biotechnol.* **1997**, *15*, 269–272.

(3) Willett, R. L.; Baldwin, K. W.; West, K. W.; Pfeiffer, L. N. *Proc. Nat. Acad. Sci. U.S.A.* **2005**, *102*, 7817–7822.

(4) Wei, Y.; Latour, R. A. *Langmuir* **2008**, *24*, 6721–6729.

(5) Peelle, B. R.; Krauland, E. M.; Wittrup, K. D.; Belcher, A. M. *Langmuir* **2005**, *21*, 6929–6933.

(6) Krauland, E. M.; Peelle, B. R.; Wittrup, K. D.; Belcher, A. M. *Biotechnol. Bioeng.* **2007**, *97*, 1009–1020.

(7) Li, H.-Q.; Chen, A.; Roscoe, Sh. G.; Lipkowski, J. *J. Electroanal. Chem.* **2001**, *500*, 299–310.

(8) Tamerler, C.; Duman, M.; Oren, E. E.; Gungormus, M.; Xiong, X.; Kacar, T.; Parviz, B. A.; Sarikaya, M. *Small* **2006**, *11*, 1372–1378.

(9) Hnilova, M.; Oren, E. E.; Seker, U. O.; Wilson, B. R.; Collono, S.; Evans, J. S.; Tamerler, C.; Sarikaya, M. *Langmuir* **2008**, *24*, 12440–12445.

(10) Tamerler, C.; Oren, E. E.; Duman, M.; Venkatasubramanian, E.; Sarikaya, M. *Langmuir* **2006**, *22*, 7712–7718.

(11) Gray, J. J. *Curr. Opin. Struct. Biol.* **2004**, *14*, 110–115.

(12) Harding, J. H.; Duffy, D. M.; Sushko, M. L.; Rodger, P. M.; Quigley, D.; Elliot, J. A. *Chem. Rev.* **2008**, *108*, 4823–4854.

(13) Latour, R. A. *Biointerphases* **2008**, *3*, FC2–FC12.

(14) Cohavi, O.; Corni, S.; De Rienzo, F.; Di Felice, R.; Gottschalk, K. E.; Höfling, M.; Kokh, D.; Molinari, E.; Schreiber, G.; Vaskevich, A.; Wade, R. C. *J. Mol. Recog.* **2010**, *23*, 259−262.

(15) Nakanashi, K.; Sakiyama, T.; Imamura, K. *Biosci. Bioing.* **2001**, *91*, 233–244.

(16) Horinek, D.; Serr, A.; Geisler, M.; Pirzer, T.; Slotta, U.; Lud, S. Q.; Garrido, J. A.; Scheibel, T.; Hugel, T.; Netz, R. R. *Proc. Nat. Acad. Sci. U.S.A.* **2008**, *105*, 2842–2847.

(17) Raut, V. P.; Agashe, M. A.; Stuart, S. J.; Latour, R. A. *Langmuir* **2005**, *21*, 1629–1639.

(18) Raffaini, G.; Ganazzoli, F. *Langmuir* **2004**, *20*, 3371–3378. Makrodimitris, K.,; Masica, D. L.; Kim, E. T.; Gray, J. J. *J. Am. Chem. Soc.* **2007**, *129*, 13713–13722.

(19) Heinz, H.; Farmer, B. L.; Pandey, R. B.; Slocik, J. M.; Patnaik, S. S.; Pachter, R.; Naik, R. R. *J. Am. Chem. Soc.* **2009**, *131*, 9704–9714.

(20) Heinz, H.; Vaia, R. A.; Farmer, B. L.; Naik, R. R. *J. Phys. Chem. C* **2008**, *112*, 17281–17290.

(21) Braun, R.; Sarikaya, M.; Schulten, K. J. *Biomater. Sci. Polymer Ed.* **2002**, *13*, 747–757.

(22) Kantarei, N.; Tamerler, C.; Sarikaya, M.; Halilogla, T.; Doruker, P. *Polymer* **2005**, *46*, 4307–4313.

(23) Ghiringhelli, L. M.; Hess, B.; van der Vegt, N. F. A.; Delle Site, L. *J. Am. Chem. Soc.* **2008**, *130*, 13460–13464.

(24) Verde, A. V.; Acres, J. M.; Maranas, J. K. *Biomacromolecules* **2009**, *10*, 2118–2128.

(25) Feig, M.; Brooks, C. L., III. *Curr. Opin. Struct. Biol.* **2004**, *14*, 217–224.

(26) Sun, Y.; Latour, R. *J. Comput. Chem.* **2006**, *27*, 1908–1922.

(27) Iori, F.; Di Felice, R.; Molinari, E.; Corni, S. *J. Comput. Chem.* **2009**, *30*, 1465–1476.

(28) Hoefling, M.; Iori F.; Corni, S.; Gottschalk, K. E. *ChemPhysChem* **2010**, [Online] DOI: 10.1002/cphc.200900981.

(29) Hoefling, M.; Iori, F.; Corni, S.; Gottschalk, K. E. *Langmuir* **2010**, in press.

(30) Gabdoulline, R. R.; Wade, R. C. *Biophys. J.* **1997**, *72*, 1917–1929.

(31) Shkel, I. A.; Kim, S. Two Dimensional Reaction of Biological Molecules Studied by Weighted Ensemble Brownian Dynamics *Proceedings of the 4th Pacific Symposium on Biocomputing*, (PSB '99) Hawaii, January 4−9, 1999; Altman, R. B., Dunker, A. K., Hunter, L., Klein, T. E., Eds. http://psb.stanford.edu/psb-online/ (accessed Apr 20, 2010); pp 468−479.

(32) Goba, C.; Geyer, T.; Helms, V. *J. Chem. Phys.* **2004**, *121*, 457–464.

(33) Tiel, P. A.; Madey, Th. E. *Surf. Sci. Rep.* **1987**, *7*, 211–285. Henderson, M. A. *Surf. Sci. Rep.* **2002**, *46*, 1–308.

(34) Meng, Sh.; Wang, E. G.; Gao, Sh. *J. Chem. Phys.* **2003**, *119*, 7617–7620. Meng, Sh.; Wang, E. G.; Gao, Sh. *Phys. Rev. B* **2004**, *69*, 195404–17.

(35) Michaelides, A.; Ranea, V. A.; de Andres, P. L.; King, D. A. *Phys. Rev. Lett.* **2003**, *90*, 216102–216106.

(36) Criscenti, L. J.; Cygan, R. T.; Kooser, A. S.; Moffat, H. K. *Chem. Mater.* **2008**, *20*, 4682–4693.

(37) Ju, Sh.-P. J. *Chem. Phys.* 2005*122*, 094718−094718−6.

(38) Chang, Ch.-I.; Lee, W.-J.; Young, T.-F.; Ju, Sh.-P.; Chang, Ch.-W.; Chen, H.-L.; Chang, J.-G. *J. Chem. Phys.* **2008**, *128*, 154703−154703−9.

(39) Torrie, G. M.; Kusalik, P. G.; Patey, G. N. *J. Chem. Phys.* **1988**, *88*, 7826–7840. Bérard, D. R.; Kinoshita, M.; Ye, X.; Patey, G. N. *J. Chem. Phys.* **1994**, *101*, 6271–6280. Bérard, D. R.; Kinoshita, M.; Ye, X.; Patey, G. N. *J. Chem. Phys.* **1995**, *102*, 1024–1033.

(40) Guidelli, R.; Schmickler, W. *Electrocheim. Acta.* **2000**, *45*, 2317–2338.

(41) Barten, D.; Kleijn, J. M.; Duval, J.; v. Leeuwen, H. P.; Lyklema, J.; Cohen Stuart, M. A. *Langmuir* **2003**, *19*, 1133–1139. Hillier, A. C.; Kim, S.; Bard, A. J. *J. Phys. Chem.* **1996**, *100*, 18808–18817.

(42) Ataka, K.; Yotsuyanagi, T.; Osawa, M. *J. Phys. Chem.* **1996**, *100*, 10664–10672. Nihonyanagi, S.; Ye, Sh.; Uosaki, K.; Dreesen, L.; Humbert, Ch.; Thiry, P.; Peremans, A. *Surf. Sci.* **2004**, *573*, 11–16.

(43) Schrader, M E. *J. Colloid Interface Sci.* **1984**, *100*, 372–380.

(44) Sendner, Ch.; Horinek, D.; Bocquet, L.; Netz, R. R. *Langmuir* **2009**, *25*, 10768–10781.

(45) Löfgren, P.; Ahlström, P.; Chakarov, D. V.; Lausmaa, J.; Kasemo, B. *Surf. Sci.* **1996**, *367*, L19–L25. Smith, R. S.; Huang, C.; Wong, E. K. L.; Kay, B. D. *Surf. Sci.* **1996**, *367*, L13–L18.

(46) Jorgensen, W. L.; Tirado-Rivers, J. *J. Am. Chem. Soc.* **1988**, *110*, 1657–1666.

(47) Iori, F.; Corni, S. *J. Comput. Chem.* **2008**, *29*, 1656–1666.

(48) Finnis, M. W. *Surf. Sci.* **1991**, *241*, 61–72. Sahni, V.; Bohnen, K.-P. *Phys. Rev. B* **1985**, *31*, 7651–7661.

(49) Gabdoulline, R. R.; Wade, R. C. *J. Phys. Chem.* **1996**, *100*, 3868–3878.

(50) Madura, J. D.; Briggs, J. M.; Wade, R. C.; Davis, M. E.; Luty, B. A.; Ilin, A.; Antosiewicz, J.; Gilson, M. K.; Bagheri, B.; Scott, L. R.; McCammon, J. A. *Comput. Phys. Commun.* **1995**, *9*, 57–95.

(51) Gabdoulline, R. R.; Wade, R. C. *Methods* **1998**, *14*, 329–341.

(52) Gabdoulline, R. R.; Wade, R. C. *J. Mol. Biol.* **1999**, *291*, 149–162.

(53) Davis, M. E. *J. Chem. Phys.* **1994**, *100*, 5149–5159.

(54) Hamann, C. H.; Hamnet, A.; Vielstich, W. *Electrochemistry*; Wiley: New York, 1998.

(55) Gabdoulline, R. R.; Wade, R. C. *J. Am. Chem. Soc.* **2009**, *131*, 9230–9238.

(56) Ben-Tal, N.; Honig, B.; Bagdassarian, C. K.; Ben-Shaul, A. *Biophys. J.* **2000**, *79*, 1180–1187.

(57) Harvey, S. C.; Prabhakaran, M. *J. Phys. Chem.* **1987**, *91*, 4799–4801.

(58) Beutler, T. C.; van Gunsteren, W. F. *J. Phys. Chem.* **1994**, *100*, 1492–1497.

(59) Hess, B.; Kutzner, C.; Van Der Spoel, D.; Lindahl, E. *J. Chem. Theory Comput.* **2008**, *4*, 435–447.

(60) Yeh, I. C.; Berkowitz, M. L. *J. Chem. Phys.* **1999**, *111*, 3155–3162.

(61) Donnini, S.; Mark, A. E.; Juffer, A. H.; Villa, A. *J. Comput. Chem.* **2005**, *26*, 115–122.

(62) Trzesniak, D.; Kunz, A.-P. E.; van Gunsteren, W. F. *ChemPhysChem* **2007**, *8*, 162–169.

(63) Kaestner, J.; Thiel, W. *J. Chem. Phys.* **2005**, *123*, 144104. Van Eerden, J.; Briels, W. J.; Harkema, S.; Feil, D. *Chem. Phys. Lett.* **1989**, *164*, 370–376.

(64) Hess, B.; Bekker, H.; Berendsen, H. J. C.; Fraaije, J. G. E. M. *J. Comput. Chem.* **1997**, *18*, 1463–1472.

(65) Sedlmeier, F.; Janecek, J.; Sedner, C.; Bocquet, L.; Netz, R. R.; Horinek, D. D. *Biointerphases* **2008**, *3*, FC23–FC39.

(66) Harris, J. G. *J. Phys. Chem.* **1992**, *96*, 5077–5086.

CT100086J